16. L. R. Moore, S. W. Chisholm, *Limnol. Oceanogr.* **44**, 628 (1999).
17. L. R. Moore *et al.*, *Limnol. Oceanogr.* **47**, 989 (2002).
18. E. Zinser *et al.*, *Appl. Environ. Microbiol.* **72**, 723 (2006).
19. N. Ahlgren *et al.*, *Environ. Microbiol.* **8**, 441 (2006).
20. N. J. West, D. J. Scanlan, *Appl. Environ. Microbiol.* **65**, 2585 (1999).
21. J. Aiken *et al.*, *Prog. Oceanogr.* **45**, 257 (2000).
22. S. B. Hooker *et al.*, *Prog. Oceanogr.* **45**, 313 (2000).
23. M. S. Rappe, S. J. Giovannoni, *Annu. Rev. Microbiol.* **57**, 369 (2003).
24. L. Campbell *et al.*, *Deep-Sea Res. Part II Top. Stud. Oceanogr.* **45**, 2301 (1998).
25. K. K. Cavender-Bares *et al.*, *Deep-Sea Res. Part I Oceanogr. Res. Pap.* **48**, 2373 (2001).
26. L. R. Moore *et al.*, *Aquat. Microb. Ecol.* **39**, 257 (2005).
27. M. B. Sullivan *et al.*, *Nature* **424**, 1047 (2003).
28. B. C. Monger *et al.*, *Limnol. Oceanogr.* **44**, 1917 (1999).
29. J. C. Venter *et al.*, *Science* **304**, 66 (2004).
30. The authors acknowledge C. Robinson and the captain and crew of Royal Research Ship *James Clark Ross* for our participation in the AMT cruise and D. Veneziano for guidance with the statistical analysis. This work was funded in part by the Gordon and Betty Moore Foundation, the Seaver Foundation, NSF Biological Oceanography Division (to S.W.C.), and U.S. Department of Energy (to S.W.C.), NOAA and the University of Hawaii (to Z.I.J.), and NSF and the University of Tennessee (to E.R.Z.). It was also supported by the UK Natural Environment Research Council through the AMT consortium (NER/O/S/2001/00680). This is School of Ocean and Earth Science and Technology contribution no. 6686 and AMT contribution no. 107.

Supporting Online Material
www.sciencemag.org/cgi/content/full/311/5768/1737/DC1
Materials and Methods
Figs. S1 to S6

27 July 2005; accepted 11 January 2006
10.1126/science.1118052

REPORTS

General Strategies for Nanoparticle Dispersion

Michael E. Mackay,[1,2]* Anish Tuteja,[1] Phillip M. Duxbury,[2] Craig J. Hawker,[3,4] Brooke Van Horn,[4] Zhibin Guan,[5] Guanghui Chen,[5] R. S. Krishnan[1]

Traditionally the dispersion of particles in polymeric materials has proven difficult and frequently results in phase separation and agglomeration. We show that thermodynamically stable dispersion of nanoparticles into a polymeric liquid is enhanced for systems where the radius of gyration of the linear polymer is greater than the radius of the nanoparticle. Dispersed nanoparticles swell the linear polymer chains, resulting in a polymer radius of gyration that grows with the nanoparticle volume fraction. It is proposed that this entropically unfavorable process is offset by an enthalpy gain due to an increase in molecular contacts at dispersed nanoparticle surfaces as compared with the surfaces of phase-separated nanoparticles. Even when the dispersed state is thermodynamically stable, it may be inaccessible unless the correct processing strategy is adopted, which is particularly important for the case of fullerene dispersion into linear polymers.

Polymer phase stability in solution (*1*) or with another polymer (*2*) has been studied for over 50 years and found to be a delicate balance of entropic and enthalpic contributions to the total free energy. For example, it is possible to fractionate a polymer by size with a small change in solvent quality (*3*) and to control miscibility of chemically identical polymers whose only difference is architecture (branching) (*4*). More recently, the phase stability of nanoparticle-polymer blends has attracted intense scrutiny (*5*) and is challenging to predict because of computational difficulty in accessing the relevant length and time scales. Flory theories, density functional theories, and molecular dynamics methods provide essential guidance, although accurate calculations are restricted to two or at most a few nanoparticles in the relevant size regime (*6*, *7*). Despite these difficulties, a vast array of applications are emerging that require nanoparticle dispersion, such as in the use of fullerenes to enhance the efficiency of polymer-based photovoltaic devices (*8*, *9*) and in the control of polymer viscosity using nanoparticles (*10*).

We demonstrate strategies for control of nanoparticle dispersion in linear polymer melts. We start with discussion of processing procedures that enable stable dispersion of fullerenes and then present an experimental characterization of the parameters that control the phase boundary between the dispersed and phase-segregated states of carefully considered nanoparticle-polymer mixtures. Moreover, it has been proven possible to disperse polyethylene nanoparticles in polystyrene despite the fact that linear polyethylene–linear polystyrene is a classic phase-separating blend, which implies that nanoparticle morphology may actually enhance dispersion. This hypothesis is tested by using a system composed of polystyrene nanoparticles dispersed in linear polystyrene, because the monomer-monomer contacts in this system are the same for all of its constituents. An enthalpic mechanism that arises from nanoparticle packing effects operates at the nanoscale and is necessary in order to understand dispersion in this size regime. A Flory theory, which includes this enthalpic contribution as well as chain stretching caused by nanoparticle dispersion and the standard mixing entropy, is used to reconcile the experimental observations and emphasize the importance of the nanoparticle-to-polymer size ratio in controlling nanoparticle dispersion.

First we discuss the dispersion of fullerenes into polystyrene, motivated by earlier work that suggested that fullerene dispersion in polymers (*11*) is poor, limiting their utility, for example, in solar cells (*8*, *9*). For a polymer blend, the insertion energy of a linear polymer chain with another controls dispersion and grows with the number of monomers in the chain. So, the insertion enthalpy of a chain of N monomers is proportional to $N\chi$, where χ is the Flory mixing parameter and is the primary cause of phase separation in incompatible blends. Nanoparticles have an insertion enthalpy that grows in proportion to the surface area of the nanoparticle, yielding an insertion enthalpy of $s \sim A\chi$, where $A = 4\pi a^2$ for a nanoparticle of radius a. Although this enhancement is not as strong as for polymer blends, dispersion of nanoparticles still depends critically on χ. We observed experimentally that it is possible to disperse up to a concentration of 2 volume % of C_{60} in linear, monodisperse polystyrene. At small nanoparticle concentration, Flory theory (*1*) gives a binodal or phase stability volume frac-

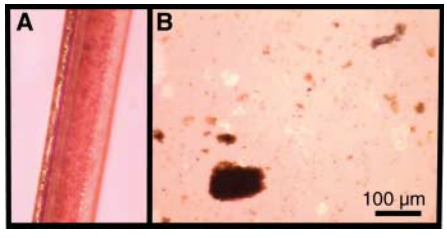

Fig. 1. (**A**) Rapid precipitation of fullerene-polystyrene blends, followed by drying and melt processing, allows manufacture of fibers. The fibers contains 1 wt % C_{60} fullerenes that were melt spun into long fibers with a diameter of circa 1 mm. (**B**) Fullerene (1 wt %)-polystyrene blends developed through regular solvent evaporation produce large, phase-separated domains, which are not apparent in the fiber.

[1]Department of Chemical Engineering and Materials Science, [2]Department of Physics and Astronomy, Michigan State University, East Lansing, MI 48824, USA. [3]Materials Research Laboratory, University of California, Santa Barbara, CA 93106, USA. [4]IBM Almaden Research Center, 650 Harry Road, San Jose, CA 95120, USA. [5]Department of Chemistry, University of California, Irvine, CA 92697, USA.

*To whom correspondence should be addressed. E-mail: mackay@msu.edu

tion (ϕ_B) of $\phi_B \approx \exp[-(1 + s)]$, assuming the phase-separated fullerenes form a pure nanoparticle phase. The use of the experimental value of $\phi_B = 0.02$ yields an insertion enthalpy per fullerene on the order of $s \approx 3$. The molecular insertion energy per monomer (ε) is given by $s = z\varepsilon/k_BT$, where z is the coordination number; k_B, the Boltzmann constant; and T, the temperature; yielding an insertion energy of $\varepsilon \approx 0.02$ eV for fullerenes in polystyrene. This relatively small energy may be rationalized by the fact that favorable molecular contacts between the aromatic rings on polystyrene and the hexagons on the surface of C_{60} may occur.

Fullerene dispersion is enabled by using our technique of rapidly precipitating the components in a mutual nonsolvent (*10*, *12*) to arrive at a dried powder that is then thermally aged, allowing melt processing and fiber spinning (Fig. 1A). It is known that fullerenes have limited solubility in organic solvents (*13*) on the order of 5 to 10 mg/ml. Solvent evaporation from a fullerene-polymer solution will lead to a fullerene supersaturated state at low overall concentration and likely phase separation (Fig. 1B). Thus, to reach the thermodynamically favored state, we had to carefully control the processing procedure for nanoparticle dispersion to avoid a kinetically trapped condition.

A more surprising result is that we observed dispersion of large branched polyethylene nanoparticles (*14*, *15*) in polystyrene (Fig. 2 and SOM). This is surprising because linear polystyrene–linear polyethylene blends (*2*) have an unfavorable mixing enthalpy and are a classic phase-separating system, with complete phase separation occurring at molecular weights typical of those used here. We have taken transmission electron microscope (TEM) images and collected small angle neutron scattering (SANS) data for a wide variety of mixtures. The TEM image (Fig. 2B) illustrates the dispersion of dendritic polyethylene nanoparticles in 393-kD linear polystyrene, from which a nanoparticle radius of 10 to 15 nm can be extracted. Moreover, a Guinier analysis of SANS data (*16*, *17*) from polyethylene nanoparticles in dilute solution yields a polyethylene-nanoparticle radius of 12.8 ± 0.1 nm, which is consistent with the TEM measurement. Neutron-scattering data for the same nanoparticles blended with linear polystyrene melts with different molecular weights are also presented (Fig. 2C). Architecture and size both make a clear difference in the miscibility of this system, because the dendritic polyethylene nanoparticles are miscible with 393-kD linear polystyrene [radius of gyration (R_g) = 17.3 nm], as evidenced by the nonfractal SANS results at small wave vector (*16*, *17*). However, miscibility does not occur when the same polyethylene nanoparticles are blended with either 155-kD (deuterated) linear polystyrene (R_g = 10.5 nm) or a smaller protonated 75-kD polystyrene (R_g = 7.5 nm), as shown (Fig. 2C). The latter experiment demonstrates that the isotope effect (*18*) is not causing phase separation; rather, the relative size of the nanoparticle and polymer is key (*19*–*21*).

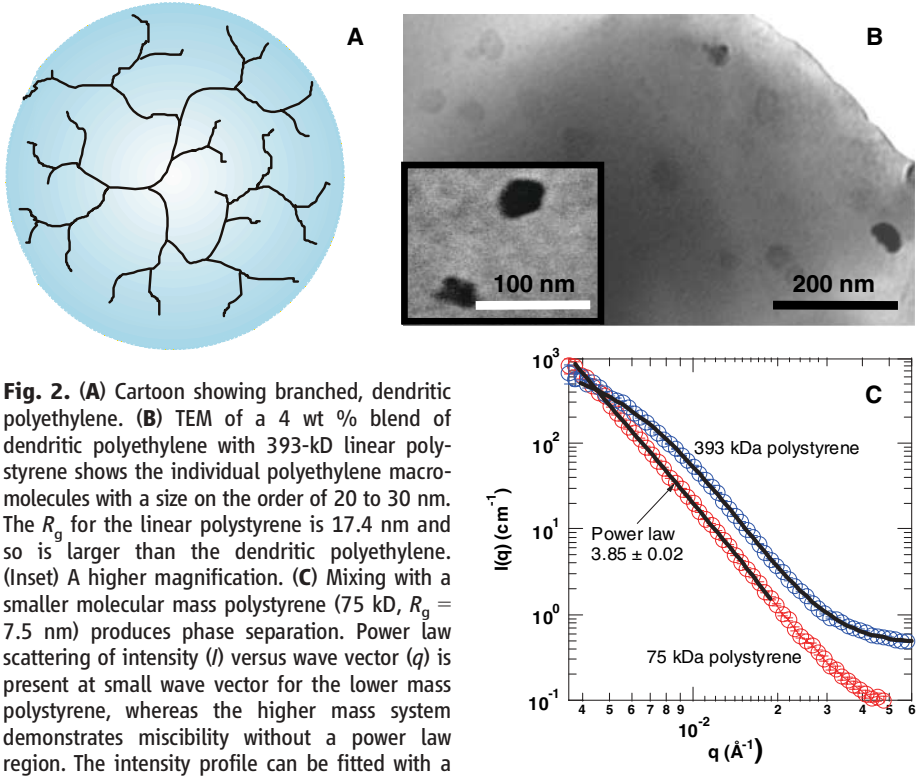

Fig. 2. (**A**) Cartoon showing branched, dendritic polyethylene. (**B**) TEM of a 4 wt % blend of dendritic polyethylene with 393-kD linear polystyrene shows the individual polyethylene macromolecules with a size on the order of 20 to 30 nm. The R_g for the linear polystyrene is 17.4 nm and so is larger than the dendritic polyethylene. (Inset) A higher magnification. (**C**) Mixing with a smaller molecular mass polystyrene (75 kD, R_g = 7.5 nm) produces phase separation. Power law scattering of intensity (I) versus wave vector (q) is present at small wave vector for the lower mass polystyrene, whereas the higher mass system demonstrates miscibility without a power law region. The intensity profile can be fitted with a polydisperse sphere model, yielding a mean radius (11.0 nm) for the dendritic polyethylene that agrees well with the TEM images.

A particularly clear illustration of the importance of the ratio a/R_g on nanoparticle dispersion is provided by a mixture consisting of cross-linked polystyrene nanoparticles (*22*) blended with linear polystyrene. We observed phase separation when the nanoparticle size was greater than the polymer radius of gyration in a manner similar to that observed in the case of polyethylene nanoparticle mixtures discussed above.

Tightly cross-linked polystyrene nanoparticles, where every fifth monomer unit is potentially cross-linked (*22*), were blended with linear polystyrene (*10*). This system produces a stable blend even when the interparticle gap reaches surprisingly small distances, suggesting the linear polystyrene molecule is highly distorted (*10*). The distortion was directly measured through a SANS Guinier analysis from a sample in which 2 weight (wt) % deuterated linear polystyrene was blended with protonated linear polystyrene of similar molecular weight and various concentrations of protonated polystyrene nanoparticles (Fig. 3A). The radius of gyration for the linear polystyrene increases with nanoparticle concentration, and the linear chains remain globular in nature, as determined through careful analysis using models that distinguish between sphere-like, rod-like, and disk-like shapes (*23*).

Chain stretching has been observed in some Monte Carlo simulations (*24*), although in many others chain contraction has been noted (*25*). Both chain expansion and chain contraction have been observed in neutron scattering from isotopically labeled polydimethylsiloxane (PDMS) blends containing silica particles (*26*). In this system, nanoparticles of radius ~ 1 nm were blended with linear polymers with a similar R_g value of ~3 to 10 nm. The polymer mixtures with smaller R_g values experienced chain contraction upon nanoparticle addition, whereas the polymer mixtures with larger R_g values experienced chain expansion with nanoparticle addition. In our system, the linear polymer R_g value was varied between 4 and 11 nm, the nanoparticle radius was about 3 nm, and we observed chain expansion in all cases (Fig. 3A). Moreover, excluded volume does not fully account for the radius increase, because, if it is assumed that the individual polymer and nanoparticle densities do not change on mixing, then the radius of gyration relative to that without nanoparticle incorporation (R_g/R_{g0}) is expected to vary as $(1 + \phi)^{1/5}$. The chain stretching is larger than the amount suggested by this relationship and is empirically close to $1 + c\phi$, with c about 1.

Despite the linear polymer distortion, we found that a large miscible region exists for cross-linked polystyrene nanoparticles blended with linear polystyrene (Fig. 3B). The data were determined from SANS through presence or absence of fractal-like scattering at small wave vector and at nanoparticle concentrations of 2 wt %. Fractal-like behavior is indicative of a non-equilibrium state consisting of irregular phase-separated aggregates, which exist on many length

scales, despite the fact that the phase separation is driven by a gain in equilibrium free energy. Data from the fullerene–linear polystyrene and polyethylene nanoparticle–linear polystyrene systems are also included in this phase diagram, indicating that this graph provides a useful guide for a range of nanocomposite systems. The experimental data demonstrate that if the linear polymer R_g is larger than the nanoparticle radius then miscibility is promoted. Note that both the polymer R_g and nanoparticle radius were experimentally determined via SANS.

To experimentally determine the Flory χ parameter, we found the second virial coefficient for 211-kD tightly cross-linked polystyrene nanoparticles dissolved in 473-kD deuterated linear polystyrene to be $5.3 \times 10^{-5} \pm 3.4 \times 10^{-5}$ cc-mol/g^2 at 127°C and $2.4 \times 10^{-5} \pm 0.6 \times 10^{-5}$ cc-mol/g^2 at 170°C by using SANS data and a Zimm analysis (*16*, *17*). A standard analysis, strictly valid for linear-linear architecture blends (*27*, *28*), yields Flory parameters of χ equal to -2.7×10^{-3} (at 127°C) and -1.2×10^{-3} (at 170°C), demonstrating that mixing is favored at both temperatures. Bates and Wignall (*18*) found χ to be $\sim 10^{-4}$ for deuterated polystyrene blends, indicating that the negative mixing enthalpy is not due to isotopic substitution. Furthermore, the χ parameter is found to follow $\sim +0.01 - 6/T$ (in K), confirming that favorable enthalpic interactions, which are geometric in origin, are responsible for the phase stability.

This unusual behavior is explained by considering the number of molecular contacts between monomers in the isolated nanoparticle state compared to that of a nanoparticle in the dispersed state, as illustrated in the idealized model (Fig. 3C). The energy gain of a monomer-monomer contact is taken to be ε_{np}. However, the van der Waals force operates over an effective distance (δ) so that only a fraction of the nanoparticle area $(A_C) = (z\delta/4a) \times A$ has this favorable molecular contact. Here, z is the average coordination number of the nanoparticle aggregate. The remaining uncovered surface area of the nanoparticle ($A_U \equiv A - A_C$) does not profit from favorable contacts with other nanoparticles. Nanoparticles may thus gain enthalpically favorable monomer-monomer contacts by dispersion in the polymer melt, as has been noted in recent polymer reference interaction site model (PRISM) calculations (*7*). Smaller nanoparticles do not experience this enthalpic driving force because A_C tends toward A in this limit, confirming that C_{60} fullerenes are miscible solely through a favorable mixing entropy.

The mixing enthalpy of a nanoparticle, s, can be related to the Flory parameter via $s = A_C\chi + A_U(\chi - \varepsilon_{np}/k_BT) \equiv s_0 - s_1$. Here $s_0 = A\chi$ is the insertion enthalpy in the absence of geometric effects due to uncovered area, and $s_1 = A_U \times \varepsilon_{np}/k_BT$ is the reduction in enthalpy within the pure nanoparticle phase due to uncovered area. The areas are expressed in lattice site dimensions and so are dimensionless, with s_0 representing the insertion energy per nanoparticle and χ that of a monomer unit. Although the uncovered area can be quite small on a given nanoparticle, the enthalpy gain via dispersion can be substantial because of their large numbers, given by ϕ/v_{np} with v_{np} being the nanoparticle volume ($^4/_3\pi a^3$). So, the expected enthalpic stabilization is given by $\phi/v_{np} \times s_1$, which exhibits a maximum at a nanoparticle radius of $z\delta/2$. This is truly a nanoscopic effect because δ is on the order of 1 nm and z is on the order of 6 for random packing (*29*), making the optimum radius for dispersion on the order of 3 nm, the size scale we have used in the present study. If the nanoparticles are too small, then solubility suffers from too little or no uncovered area to achieve sufficient enthalpic gain, similar to that experienced by the fullerenes, whereas a system containing larger particles has a reduced mixing enthalpy by a reduction in nanoparticle number for a given volume fraction.

The above argument hinges on uncovered area developed by rigid particles (Fig. 3C) and is related to an increase in the cohesive energy of a material from its pure state. The dendritic polyethylene nanoparticle system is a liquid at room temperature, and so application of the cartoon to this system is suspect. However, by using SANS of thermally annealed samples we measured the virial coefficient for this molecule dissolved in 393-kD linear polystyrene to be $2.1 \times 10^{-5} \pm 1.7 \times 10^{-5}$ cm^3 mol/g^2 at room temperature, yielding $\chi = -1.7 \times 10^{-3} \pm 1.3 \times 10^{-3}$. Again a negative mixing enthalpy is found. This result is rationalized first by noting the density of this material was determined to be quite small, 0.81 ± 0.02 g/cm^3, compared with the linear polyethylene amorphous density extrapolated to room temperature (*30*), 0.86 to 0.89 g/cm^3. Secondly, the melt surface tension (*31*, *32*) at 160°C was measured and found to be ≈30% lower than that for polyethylene of similar molecular weight (mass of 236 kD). Both these results point to a reduced internal energy in the isolated nanoparticle melt by using the semi-empirical relation between the surface tension (ST) and the cohesive energy density (CED, internal energy per unit volume); ST is about CED$^{2/3}$ (*33*) and is consistent with the enthalpy gain on mixing discussed above (i.e., negative χ).

We generalized our observations by using a Flory lattice theory that has proven useful in

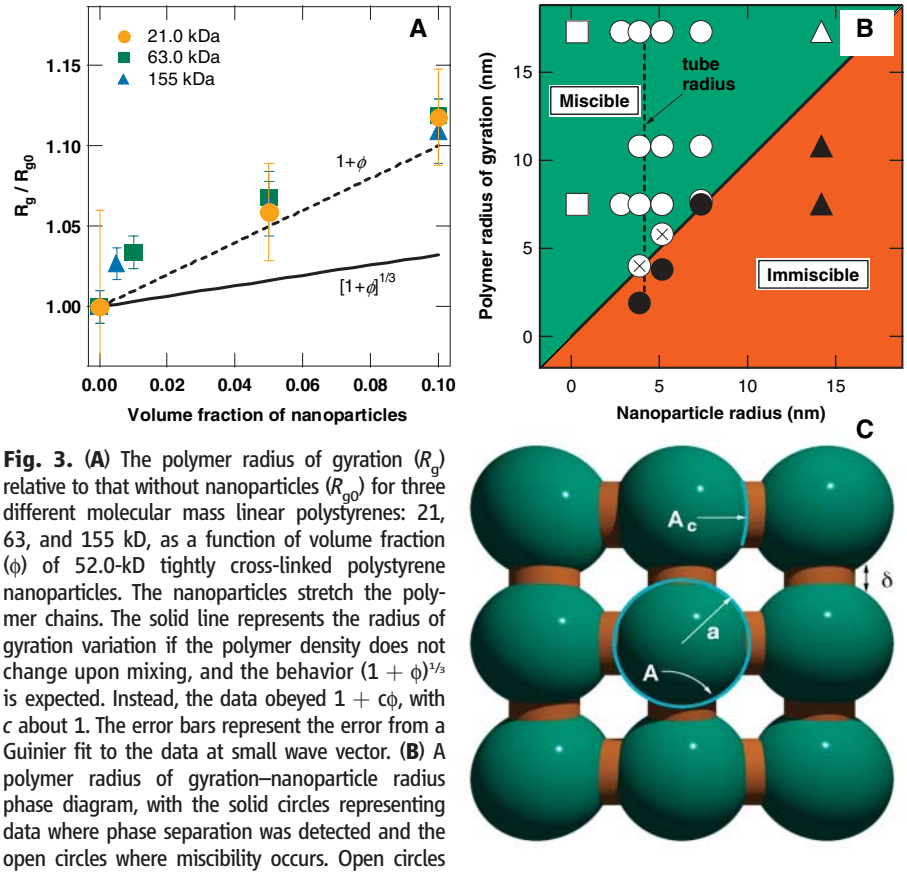

Fig. 3. (**A**) The polymer radius of gyration (R_g) relative to that without nanoparticles (R_{g0}) for three different molecular mass linear polystyrenes: 21, 63, and 155 kD, as a function of volume fraction (ϕ) of 52.0-kD tightly cross-linked polystyrene nanoparticles. The nanoparticles stretch the polymer chains. The solid line represents the radius of gyration variation if the polymer density does not change upon mixing, and the behavior $(1 + \phi)^{1/3}$ is expected. Instead, the data obeyed $1 + c\phi$, with c about 1. The error bars represent the error from a Guinier fit to the data at small wave vector. (**B**) A polymer radius of gyration–nanoparticle radius phase diagram, with the solid circles representing data where phase separation was detected and the open circles where miscibility occurs. Open circles with an × represent conditions where some agglomeration was detected by SANS yet large-scale phase separation was not observed. Squares are the C_{60}-polystyrene system; circles, the polystyrene nanoparticle–polystyrene system; and triangles, the dendritic polyethylene–polystyrene system. The dashed line represents the reptation tube radius, suggesting phase stability does not depend on the entanglement structure. The nanoparticle fraction used to generate each data point was 2 wt %. (**C**) Cartoon illustrating that the attraction between pure nanoparticles is effective only over a fraction (A_C) of the available surface area (A) because of the limited range (δ) over which dispersion forces operate.

interpreting the phase morphology of complex systems such as nanoparticle dispersion in polymer blends, where reasonable agreement with lattice density functional theory has been demonstrated (*19*). The first free energy term considered is the mixing entropy described by $F_m/Vk_BT = [\phi\log(\phi)]/v_{vp} + [(1-\phi)\log(1-\phi)]/N$, where F_m is the entropic gain due to mixing; N, the number of monomers in the linear polymer; and V, the sample volume. Polymer chain expansion (Fig. 3A) yields a loss of entropy, and so a "stretching" free energy cost (F_s) for each molecule (*34*, *35*) is included and approximated by $F_s/Vk_BT = {}^3/_2(1-\phi)(R_g{}^2/R_{g0}{}^2 - 1)/N$. Previous work (*21*, *36*) has used a chain stretching term that has its basis in the analysis of polymer brushes, which does not show as large an R_g variation with ϕ as we see experimentally. Combining the above terms, including the enthalpy of mixing discussed above, we find that

$$v_{np}F/Vk_BT = s\phi(1-\phi) + \phi\log(\phi) + t(1-\phi)\log(1-\phi) + {}^3/_2t(1-\phi)(R_g{}^2/R_{g0}{}^2 - 1) \quad (1)$$

where $t = v_{np}/N$, which in terms of experimentally accessible parameters is $t = (a/R_{g0})^3\rho/\rho_0$, where ρ is the bulk density of the linear polystyrene melt, and ρ_0 is the density associated with one chain in the bulk polystyrene melt (i.e., the density of a single chain based on its R_g and molecular weight). The fact that t increases as the cube of the size ratio a/R_{g0} implies that the stretching term is very unfavorable for $a > R_{g0}$, which is the basic reason why large nanoparticles do not disperse, although this may not be generalized to colloidal systems where other physics comes into play (*37*).

For the case of polystyrene nanoparticles in a linear polystyrene melt, we estimate the effect of the linear polymer stretch, the third term in Eq. 1, by using the data of Fig. 3A approximated by $R_g/R_{g0} \approx 1 + c\phi$. By setting the first and second derivatives of Eq. 1 with respect to ϕ to zero, one finds the binodal at $\phi_B = \exp\{-[1 + s + (3c-1)t]\} = \exp\{-[1 + s + (3c-1)(\rho/\rho_1)(a/R_{g0})^3]\}$ and the spinodal at $\phi_s = 1/[2s + (6c - 3c^2 - 1)t]$ for small ϕ. In Ginzburg's work (*21*), an addition nonideal term, the Carnahan-Starling term, is used to assess interaction effects between nanoparticles that do not alter the binodal at small concentration. Validity of the model is confirmed by calculating s from the predicted binodal concentration, assuming c is 1 (Fig. 3A). Further, letting a/R_{g0} be 1 to delineate the phase boundary (Fig. 3B) and calculating $\rho/\rho_0 (= 1.7 \times \sqrt{M})$ for polystyrene (M is molecular mass in kD), then s values of –15 and –64 for molecular masses of 30 kD (R_{g0} = 5 nm) and 320 kD (R_{g0} = 15 nm), respectively, are determined. Dividing these values by the nanoparticle area results in χ on the order of -3×10^{-3}, in good agreement with the values determined above via neutron scattering.

References and Notes

1. P. J. Flory, *Principles of Polymer Chemistry* (Cornell Univ. Press, Ithaca, NY, 1953), p. 672.
2. L. A. Utracki, *Polymer Alloys and Blends* (Hanser, New York, 1990), p. 356.
3. L. H. Cragg, H. Hammerschlag, *Chem. Rev.* **39**, 79 (1946).
4. L. A. Utracki, B. Schlund, *Polym. Eng. Sci.* **27**, 1512 (1987).
5. Y. Lin *et al.*, *Nature* **434**, 55 (2005).
6. J. B. Hooper, K. S. Schweizer, T. G. Desai, R. Koshy, P. Keblinski, *J. Chem. Phys.* **121**, 6986 (2004).
7. J. B. Hooper, K. S. Schweizer, *Macromolecules* **38**, 8858 (2005).
8. N. S. Sariciftci, L. Smilowitz, A. J. Heeger, F. Wudl, *Science* **258**, 1474 (1992).
9. N. S. Sariciftci, A. J. Heeger, *Synth. Met.* **70**, 1349 (1995).
10. M. E. Mackay *et al.*, *Nat. Mater.* **2**, 762 (2003).
11. D. Weng *et al.*, *Eur. Polym. J.* **35**, 867 (1999).
12. F. M. Du, J. E. Fischer, K. I. Winey, *J. Poly Sci. Part B* **41**, 3333 (2003).
13. V. N. Bezmel'nitsyn, A. V. Eletskii, *Usp. Fiz. Nauk* **41**, 1091 (1998).
14. Z. Guan, P. M. Cotts, E. F. McCord, S. J. McLain, *Science* **283**, 2059 (1999).
15. Z. B. Guan, *J. Poly Sci. Part A* **41**, 3680 (2003).
16. S. M. King, in *Modern Techniques for Polymer Characterisation*, R. A. Pethrick, J. V. Dawkins, Eds. (Wiley, New York, 1999).
17. J. S. Higgins, H. C. Benoît, *Polymers and Neutron Scattering* (Clarendon Press, Oxford, 2002), p. 436.
18. F. S. Bates, G. D. Wignall, *Phys. Rev. Lett.* **57**, 1429 (1986).
19. V. Lauter-Pasyuk *et al.*, *Physica B* (Amsterdam) **248**, 243 (1998).
20. R. B. Thompson, V. V. Ginzburg, M. W. Matsen, A. C. Balazs, *Science* **292**, 2469 (2001).
21. V. V. Ginzburg, *Macromolecules* **38**, 2362 (2005).
22. E. Harth *et al.*, *J. Am. Chem. Soc.* **124**, 8653 (2002).
23. J. M. Gallas, K. C. Littrell, S. Seifert, G. W. Zajac, P. Thiyagarajan, *Biophys. J.* **77**, 1135 (1999).
24. M. A. Sharaf, J. E. Mark, *Polymer* **45**, 3943 (2004).
25. M. Vacatello, *Macromolecules* **35**, 8191 (2002).
26. A. I. Nakatani, W. Chen, R. G. Schmidt, G. V. Gordon, C. C. Han, *Polymer* **42**, 3713 (2001).
27. W. A. Kruse, R. G. Kirste, J. Haas, B. J. Schmitt, D. J. Stein, *Makrom. Chem.* **177**, 1145 (1976).
28. T. P. Russell, R. S. Stein, *J. Poly Sci.* **20**, 1593 (1982).
29. C. S. O'Hern, L. E. Silbert, A. J. Liu, S. R. Nagel, *Phys. Rev. E* **68**, 011306 (2003).
30. P. Zoller, D. J. Walsh, *Standard Pressure-Volume-Temperature Data for Polymers* (Technomic, Lancaster, PA, 1995), p. 412.
31. G. T. Dee, B. B. Sauer, *J. Colloid Inter. Sci.* **152**, 85 (1992).
32. M. E. Mackay, G. Carmezini, B. B. Sauer, W. Kampert, *Langmuir* **17**, 1708 (2001).
33. D. W. van Krevelen, *Properties of Polymers, Their Estimation and Correlation with Chemical Structure* (Elsevier, New York, ed. 2, 1976), p. 620.
34. G. Marrucci, *Trans. Soc. Rheol.* **16**, 321 (1972).
35. S. Y. Park, C. J. Barrett, M. F. Rubner, A. M. Mayes, *Macromolecules* **34**, 3384 (2001).
36. J. Huh, V. V. Ginzburg, A. C. Balazs, *Macromolecules* **33**, 8085 (2000).
37. W. C. K. Poon, *J. Phys. Cond. Matter* **14**, R859 (2002).

38. Supported by NSF DMR-0520415, NSF CTS-0400840, NSF NIRT-0210247, NSF-CTS-0417640, NSF NIRT-0506309, U.S. Department of Energy DE-FG02-90ER45418, DE-FG02-05ER46211, U.S. Department of the Army, ARO W911NF-05-1-0357, NSF DMR-0135233 (Z.G. CAREER), NSF CHEM-0456719, ARO DAAD19-01-1-0686, and the U.S. Department of Energy, Basic Energy Sciences–Materials Science, under contract W-31-109-ENG-38 to the University of Chicago. We thank P. Thiyagarajan, D. Wozniak, and developers of data reduction routines at Argonne National Laboratory in gathering and analyzing the neutron scattering data; C. Popeney and D. Camacho for their help in synthesis of the dendritic polyethylene; D. Bohnsack for its characterization; A. Pastor for help with TEM; A. Frischknecht for valuable input on this work; K. Schweizer for illuminating discussions and suggesting that we should have a negative mixing enthalpy (χ parameter) to be consistent with the observed dispersion; and E. McGarrity for help with the figures.

Supporting Online Material

www.sciencemag.org/cgi/content/full/311/5768/1740/DC1
Materials and Methods
References

4 November 2005; accepted 18 January 2006
10.1126/science.1122225

Microheterogeneity of Singlet Oxygen Distributions in Irradiated Humic Acid Solutions

Douglas E. Latch and Kristopher McNeill*

Singlet oxygen ($^1O_2$) is a highly reactive species formed through solar irradiation of organic matter in environmental waters. Implicated in a range of reactions, it has proven difficult to quantify its spatial distribution in natural waters. We assessed the microheterogeneous distribution of $^1O_2$ in irradiated solutions containing chromophoric dissolved organic matter (CDOM) by using molecular probes of varying hydrophobicity. The apparent $^1O_2$ concentrations ($[^1O_2]_{app}$), measured by recently developed hydrophobic trap-and-trigger chemiluminescent probe molecules, were orders of magnitude higher than those measured by the conventional hydrophilic probe molecule furfuryl alcohol. The differential $[^1O_2]_{app}$ values measured by these probes reflect a steep concentration gradient between the CDOM macromolecules and the aqueous phase. A detailed kinetic model based on the data predicts probabilistic $^1O_2$ distributions under different solvent conditions.

Singlet oxygen ($^1O_2$), or molecular oxygen that is in its first electronic excited state ($^1\Delta_g$), has been known to be photochemically produced in natural waters since the work of Zepp *et al*. in 1977 (*1*). It is formed through interaction of dissolved oxygen with excited